Pure Appl. Geophys. 168 (2011), 2167–2179

DOI 10.1007/s00024-011-0298-y

Pure and Applied Geophysics

Singular Elasto-Static Field Near a Fault Kink

Rodrigo Arias,[1] Raúl Madariaga,[2] and Mokhtar Adda-Bedia[3]

Abstract—We study singular elastic solutions at an angular corner left by a crack that has kinked. We have in mind a geophysical context where the faults on either side of the kink are under compression and are ready to slip, or have already slipped, under the control of Coulomb friction. We find separable static singular solutions that are matched across the sides of the corner by applying appropriate boundary conditions. In our more general solution we assume that one of the sides of the corner is about to slide, i.e. it is just contained by friction, and the other may be less pressured. Our solutions display power law behaviour with real exponents that depend continuously on the angle of the corner, the coefficient of static friction and the difference of shear load on both sides of the corner. When friction is the same on both sides of the kink, the solutions split into a symmetric and an antisymmetric solution. The antisymmetric solution corresponds to the simple shear case; while the symmetric solution appears when the kink is loaded by uniaxial stress along the bisector of the kink. The antisymmetric solution is ruled out under this model with contact since the faults cannot sustain tension. When one side of the corner is less pressured one can also distinguish modes with contact overall from others that must open up on one side. These solutions provide an insight into the stress distributions near fault kinks, they can also be used as tools for improving the numerical calculation of kinks under static or dynamic loads.

1. Introduction

Kinks and other geometrical discontinuities play an essential role in the control of rupture propagation along natural faults as discussed by Sibson (1985) and many others. The study of rupture propagation along a seismic fault containing one or more kinks, jogs, bends or discontinuities has been examined by many authors (see, e.g., Segal and Pollard, 1980; King and Nabelek, 1985; Harris and Day, 1999; Poliakov *et al*., 2002; Kame and Yamashita, 1999;Kame *et al*., 2003). Most of those studies did not explicitly address the problem of the stress distribution near the kink or bend because the main concern was the study of rupture propagation. The stress field left by fracture propagation that has kinked plays a fundamental role in the energy balance of the fault, it will produce strong radiation and could stop or favor rupture propagation.

The first study of the mechanical problems posed by a kink or bend in active faults was presented by Andrews (1989) in the static approximation. He realized that kinks posed a geometrical problem and they could not remain stable under finite deformation. He then modeled a particular example of a kink and found that stresses became singular at the cusp. Following this study, many authors have examined the role of kinks on faulting from different perspectives. In the static approximation a major step was accomplished by Tada and Yamashita (1997), who found that the tip of the kink produced a stress singularity that depended on the way the tip was smoothed. In the dynamic approximation, a propagating shear crack fault with kinks has been modeled by Oglesby *et al*. (2003); Aochi *et al*. (2000) and many others.

In the dynamic approximation most of the work has been numerical, but in many of these simulations the approximation of the stress field and the boundary conditions in the immediate vicinity of the kink poses problems. Adda-Bedia and Arias (2003) and Adda-Bedia and Madariaga (2008) solved the problem of a Mode III crack propagating along a fault that has a kink. They showed that the solution of this problem was intimately related to the singularity of the static stress field in the vicinity of the kink. The static problem for the antiplane kink was solved by Sih (1965) using the eigenvalue methods proposed by

[1] Departamento de Física, FCFM, Universidad de Chile, Santiago, Chile. E-mail: rarias@dfi.uchile.cl
[2] Laboratoire de géologie, CNRS-École Normale Supérieure, Paris, France. E-mail: madariag@geologie.ens.fr
[3] Laboratoire de physique statistique, CNRS-École Normale Supérieure, Paris, France. E-mail: adda@lps.ens.fr

Williams (1952). For the in-plane or Mode II faults, the problem of the stress and displacement distribution does not seem to have been discussed in the literature except for the previous cited works by Andrews (1989) and Tada and Yamashita (1997).

In this paper we study a Mode II shear crack that has a kink at its center. When the crack abruptly changes its direction of propagation, it leaves behind a corner region that plays a characteristic role in the global elastic behavior. It is pertinent to study the nature of the elastic fields in this region since one expects the fields may develop singular behavior that is interesting by itself, and also because numerical simulations in geometries with these corners require knowledge of singular behaviors in order to be accurate and efficient.

We approach the problem of finding all possible singular and regular elastic solutions in the region close to these corners in an isotropic homogeneous elastic medium. We have in mind kinks that occur in seismic contexts, i.e. the corner sides are in contact and under compression. This raises the issue of the role of friction on the elastic solutions: we will explore static solutions in which at least one of the sides of the corner is about to give way under the prevailing local shear. We found singular power law solutions in the regions of the corner that have real exponents. The latter exponents depend continuously on the angle of the corner, the coefficient of friction and the degree of stress of the side of the corner that may not be about to give way. These exponents are universal in the sense that they depend on the elastic properties of the medium.

The seminal paper in the study of elastic angular corners is the one of Williams (1952), where he studied an angular corner with free sides, finding a solution separable in polar coordinates. Here, we use analogous solutions by Seweryn and Molski (1996) as starting points (they studied angular corners under various boundary conditions), and we match solutions of these types on both sides of the kink corner by use of appropriate boundary conditions.

2. *Singular Elastic Fields at Kinks*

We consider a Mode II shear crack with a kink and we will focus at the corner region. The geometry is shown in Fig. 1. The crack separates two infinite homogeneous elastic wedges with identical elastic properties. Since we are interested in the stress field in the vicinity of the cusp we consider that the two faults on the side of the kink extend to infinity. In the cusp of the kink we impose no smoothing. In the terminology of Barenblatt (1996) this is the intermediate asymptotic solution to the two wedges in frictional contact across the fault. Although we will not do this, the near cusp asymptotic field can be studied using a local approximation (see Tada and Yamashita, 1997). In wedge 1 we use a coordinate system (r, θ) centered on the bisector to the kink (θ increases anti-clockwise), and on wedge 2 we use a coordinate system (r, ϕ), in which ϕ increases clockwise (see Fig. 1). The fault is assumed to be in

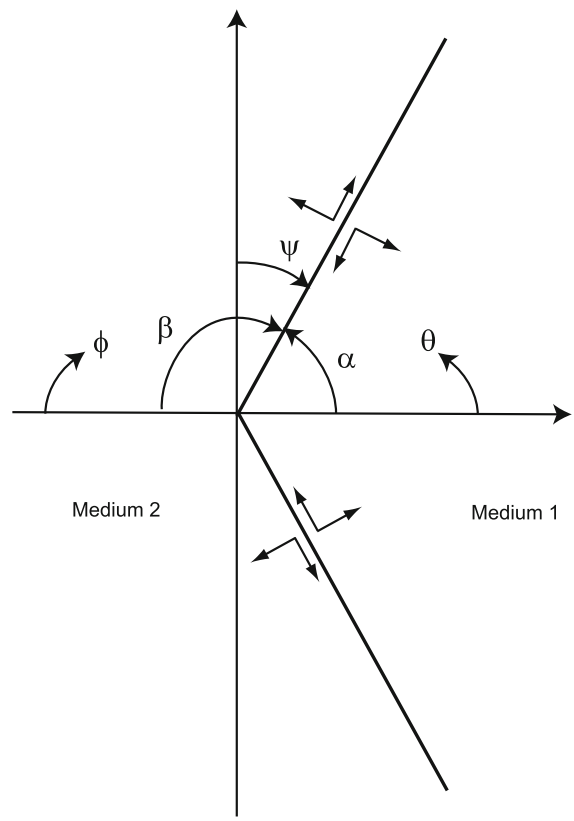

Figure 1
Geometry of a shear crack with a kink. In *medium 1*, to the *right*, we use a coordinate system (r, θ). In *medium 2*, to the *left*, we use a coordinate system (r, ϕ). The two media are in frictional contact at $\theta = \alpha$, $\phi = \beta$ (as well as at $\theta = -\alpha$, $\phi = -\beta$), so that $\alpha = \pi - \beta$

contact, such that it can slip but it can not open. Displacements along the fault are given by u_r, and slip by the jump in u_r across the fault. In general u_r has different values on the two sides of the fault.

2.1. Equilibrium Equations

The elastic body is in static equilibrium, thus in absence of body forces the equilibrium equations in Cartesian coordinates are $\partial\sigma_{ij}/\partial x_j = 0$, with σ_{ij} the different components of the stress tensor field. The stress and strain components (ϵ_{pq}) for this linear elastic medium are related through the elastic constants, i.e. $\sigma_{ij} = C_{ijpq}\epsilon_{pq}$. Furthermore, we consider an isotropic elastic medium, i.e. $C_{ijpq} = L\delta_{ij}\delta_{pq} + \mu(\delta_{ip}\delta_{jq} + \delta_{iq}\delta_{jp})$, with L and μ the Lamé constants. In polar coordinates the strain components are given by:

$$\epsilon_{rr} = \frac{\partial u_r}{\partial r}, \quad \epsilon_{\theta\theta} = \frac{1}{r}\frac{\partial u_\theta}{\partial \theta} + \frac{u_r}{r}, \quad \epsilon_{r\theta} = \frac{1}{r}\frac{\partial u_r}{\partial \theta} + \frac{\partial u_\theta}{\partial r} - \frac{u_\theta}{r} \tag{1}$$

The stress and strain components in polar coordinates are related through:

$$\sigma_{rr} = L(\epsilon_{rr} + \epsilon_{\theta\theta}) + 2\mu\epsilon_{rr}, \quad \sigma_{r\theta} = \mu\epsilon_{r\theta}, \quad \sigma_{\theta\theta} = L(\epsilon_{rr} + \epsilon_{\theta\theta}) + 2\mu\epsilon_{\theta\theta} \tag{2}$$

Thus, the equilibrium equations in polar coordinates, and in absence of body forces, are:

$$0 = \frac{\partial\sigma_{rr}}{\partial r} + \frac{1}{r}\frac{\partial\sigma_{r\theta}}{\partial\theta} + \frac{\sigma_{rr} - \sigma_{\theta\theta}}{r} \tag{3}$$

$$0 = \frac{\partial\sigma_{r\theta}}{\partial r} + \frac{1}{r}\frac{\partial\sigma_{\theta\theta}}{\partial\theta} + \frac{2}{r}\sigma_{r\theta} \tag{4}$$

2.2. Boundary Conditions

At the corner two elastic sides of the same type meet, and we assume that they are in contact under normal pressure (we have in mind cracks that are faults in a geophysical context). Thus, we will consider that the normal displacement, normal and shear stresses are continuous across the crack:

$$u_\phi(r, \phi = \pm\beta) = -u_\theta(r, \theta = \pm\alpha) \tag{5}$$

$$\sigma_{r\phi}(r, \pm\beta) = -\sigma_{r\theta}(r, \pm\alpha) \tag{6}$$

$$\sigma_{\phi\phi}(r, \phi = \pm\beta) = \sigma_{\theta\theta}(r, \theta = \pm\alpha) \tag{7}$$

[$\sigma_{\phi\phi}(r, \pm\beta)$ and $\sigma_{\theta\theta}(r, \pm\alpha)$ are thus assumed negative]. These are six boundary conditions independent of friction.

Furthermore, we will consider boundary conditions associated with friction, which in a general homogeneous form can be written as:

$$\sigma_{r\theta}(r, \alpha) = wf\sigma_{\theta\theta}(r, \alpha) = -\sigma_{r\phi}(r, \beta) = wf\sigma_{\phi\phi}(r, \beta) \tag{8}$$

$$\sigma_{r\theta}(r, -\alpha) = f\sigma_{\theta\theta}(r, -\alpha) = -\sigma_{r\phi}(r, -\beta) = f\sigma_{\phi\phi}(r, -\beta). \tag{9}$$

For the boundary conditions, we adopted a Coulomb model for friction in a homogeneous static version, so that the magnitude of the shear stress in the regions of contact is less than or equal to the coefficient of static friction (in this case it is named f) times the normal stress, and its direction is given by considerations of global static equilibrium and in the sense of opposing sliding. We have introduced the factor $w(|w| \leq 1)$ in order to write equations consistent with the previous statements (we have not considered spatial dependence of w for reasons of simplicity, expecting to capture the main features of solutions under friction). Furthermore, we have considered that the bottom side of the corner of Fig. 1 (corresponding to $\phi = -\beta$ and $\theta = -\alpha$) is about to slide, and the other may be in an arbitrary condition as far as the friction shear stress is concerned. We allow the factor w to vary between -1 and 1. When $w = -1$ we have the case of a kinked crack where stress on both sides of the kink is the same. When $w = 0$ the upper side of the kink (see Fig. 1) is at zero shear stress independently of the normal stress, this corresponds to a frictionless crack. When $w = 1$ the upper side is getting ready to slip in the opposite direction to that of the bottom limb.

Notice that Eqs. 8 and 9 are two independent equations only (we used the boundary conditions independent of friction in order to show that the relation between normal and shear stresses on both sides of the fault are not independent).

2.3. Singular Solutions

Next, we look for singular solutions on both sides of the corners that are matched through the previous boundary conditions. These solutions are separable,

with radial power law behaviour, and sinusoidal angular behaviour, and correspond to the fundamental solutions originally proposed by WILLIAMS (1952) (of the type $u_r = r^{\lambda}h(\theta)$ and $u_\theta = r^{\lambda}g(\theta)$, with λ and exponent to be determined). The particular version of the potentials that we use are those of SEWERYN and MOLSKI (1996). These solutions for the displacement and stress fields, close to the corner and for the elastic medium (1) to the right are written as:

$$\begin{aligned} u_r = r^{\lambda}[&A\cos((1+\lambda)\theta) + B\sin((1+\lambda)\theta) \\ &+ C\cos((1-\lambda)\theta) + D\sin((1-\lambda)\theta)] \end{aligned} \tag{10}$$

$$\begin{aligned} u_\theta = r^{\lambda}[&B\cos((1+\lambda)\theta) - A\sin((1+\lambda)\theta) \\ &+ v_2 D\cos((1-\lambda)\theta) - v_2 C\sin((1-\lambda)\theta)] \end{aligned} \tag{11}$$

$$\begin{aligned} \sigma_{\theta\theta} = r^{\lambda-1}\mu[&-2\lambda A\cos((1+\lambda)\theta) - 2\lambda B\sin((1+\lambda)\theta) \\ &- (1+\lambda)(1-v_2)C\cos((1-\lambda)\theta) \\ &- (1+\lambda)(1-v_2)D\sin((1-\lambda)\theta)] \end{aligned} \tag{12}$$

$$\begin{aligned} \sigma_{r\theta} = r^{\lambda-1}\mu[&2\lambda B\cos((1+\lambda)\theta) - 2\lambda A\sin((1+\lambda)\theta) \\ &+ (1-\lambda)(1-v_2)D\cos((1-\lambda)\theta) \\ &- (1-\lambda)(1-v_2)C\sin((1-\lambda)\theta)] \end{aligned} \tag{13}$$

And similarly, on medium (2) to the left side:

$$\begin{aligned} u_r = r^{\lambda}[&a\cos((1+\lambda)\phi) + b\sin((1+\lambda)\phi) \\ &+ c\cos((1-\lambda)\phi) + d\sin((1-\lambda)\phi)] \end{aligned} \tag{14}$$

$$\begin{aligned} u_\phi = r^{\lambda}[&b\cos((1+\lambda)\phi) - a\sin((1+\lambda)\phi) \\ &+ v_2 d\cos((1-\lambda)\phi) - v_2 c\sin((1-\lambda)\phi)] \end{aligned} \tag{15}$$

$$\begin{aligned} \sigma_{\phi\phi} = r^{\lambda-1}\mu[&-2\lambda a\cos((1+\lambda)\phi) - 2\lambda b\sin((1+\lambda)\phi) \\ &- (1+\lambda)(1-v_2)c\cos((1-\lambda)\phi) \\ &- (1+\lambda)(1-v_2)d\sin((1-\lambda)\phi)] \end{aligned} \tag{16}$$

$$\begin{aligned} \sigma_{r\phi} = r^{\lambda-1}\mu[&2\lambda b\cos((1+\lambda)\phi) - 2\lambda a\sin((1+\lambda)\phi) \\ &+ (1-\lambda)(1-v_2)d\cos((1-\lambda)\phi) \\ &- (1-\lambda)(1-v_2)c\sin((1-\lambda)\phi)] \end{aligned} \tag{17}$$

with μ the shear modulus, $v = L/(2(L+\mu))$ Poisson's ratio, L Lamé's first parameter, $v_2 \equiv (3+\lambda-4v)/(3-\lambda-4v)$, and λ an exponent to be determined by the boundary conditions as well as the different coefficients A, B, C, D, a, b , c , d (except for a constant factor, since these are linear solutions).

The boundary condition Eqs. 5–9 are effectively eight homogeneous equations for the eight unknown coefficients A, B, C, D, a, b , c , d. Thus, they have non zero solutions only for specific values of the singular exponent λ. In principle the eigenvalue equation for λ could be obtained by imposing that the corresponding 8×8 determinant to be null. But, due to symmetry considerations and other algebraic simplifications it is better to proceed otherwise: the details on how this eigenvalue equation (Eq. 55) is derived are left to the Appendix.

Next we reproduce the just mentioned eigenvalue equation, Eq. 55:

$$\begin{aligned} 0 = &4\cos^2(\lambda\pi) + [f(w+1)(1+\lambda)\sin(2\Psi)\cos(2\Psi\lambda)]^2 \\ &- [2\cos(2\Psi)\cos(2\Psi\lambda) - 2\lambda\sin(2\Psi)\sin(2\Psi\lambda) \\ &+ f(1-w)(1+\lambda)\sin(2\Psi)\cos(2\Psi\lambda)]^2, \end{aligned} \tag{18}$$

where $\Psi \equiv (\beta-\alpha)/2$. This is an eigenvalue equation for the determination of the power-law exponent λ, it takes the form $0 = g(\lambda, \Psi, f, w)$. For each value of the parameters, i.e. angle Ψ, weight w and coefficient of friction f, there is an infinite family of generally complex eigenvalues (we inferred this by using the method introduced in Sect. 2.5). Its solutions turn out to be real in the range of λ of more interest: the most singular eigenvalues in the range $0.5 \leq Re(\lambda) < 1$. In general, when $Re(\lambda) \geq 1$ the stress and displacement fields are regular, when $Re(\lambda) < 0.5$ the stress field in the vicinity of the kink has a strain energy concentration that could only be produced by an external source located at the cusp; while for $Re(\lambda) = 0.5$ the cusp behaves like a crack that stores a finite amount of energy in its neighborhood. Thus, we will analyze solutions in the range $0.5 \leq Re(\lambda) < 1$. However, there are some works where the region close to the tip has been modeled (e.g. plasticity, nonlinear elasticity) and this may allow for higher order singularities (see, e.g., LABOSSIERE and DUNN, 2001, BOUCHBINDER *et al.*, 2009).

2.4. Special Cases

The special cases that we will present, i.e. the frictionless corner and the case in which both sides

are about to slide, correspond to cases in which the matrix of the eigenvalue equation (52) is diagonal.

2.4.1 Special Case, the Frictionless Corner

If the kink slips without friction, $f = 0$ in Eqs. 8 and 9. In this case the normal and shear stresses on the sides of the kink are independent and we can assume that shear stresses drop to zero independently of normal stresses (an arbitrary continuous stress field that satisfies the equilibrium conditions and that has zero shear stress on the faults can be superimposed on top of the solution we investigate here). We study the frictionless kink in detail because it illustrates the origin of the stress field in the vicinity of the kink.

In the absence of friction ($f = 0$), the eigenfunctions separate into two separate families. One solution is symmetric about the bisector of the kink (x axis of Fig. 1), and the other is antisymmetric. They are shown schematically in Fig. 2 with loads that may originate them. The antisymmetric solution occurs on a kinked crack loaded by a pure shear stress so that shear stress and slip are antisymmetric in the two branches of the kink as shown on the left of Fig. 2. The symmetric case occurs when both branches slip in opposite directions at the cusp of the kink, as shown on the right hand side of the figure. In this case the shear stress is also symmetric. The straight shear crack, shown at the top is the limit when $\alpha \to \pi/2$ (or $\Psi \to 0$) of the antisymmetric crack. In that limit the stress field is uniform for the symmetric case.

When $f = 0$ the eigenvalue equation (55) splits in two because the off diagonal terms of the matrix in Eq. 52 are zero. The eigenvalue equation for symmetric modes can be obtained from the matrix equation (52) when only $\tilde{C} \neq 0$, and its associated exponent solves the following equation:

$$0 = \cos(\lambda\pi) + \cos(2\Psi)\cos(2\Psi\lambda) - \lambda\sin(2\Psi)\sin(2\Psi\lambda). \tag{19}$$

These are symmetric modes, with corresponding radial displacement fields in mediums 1 and 2 given by:

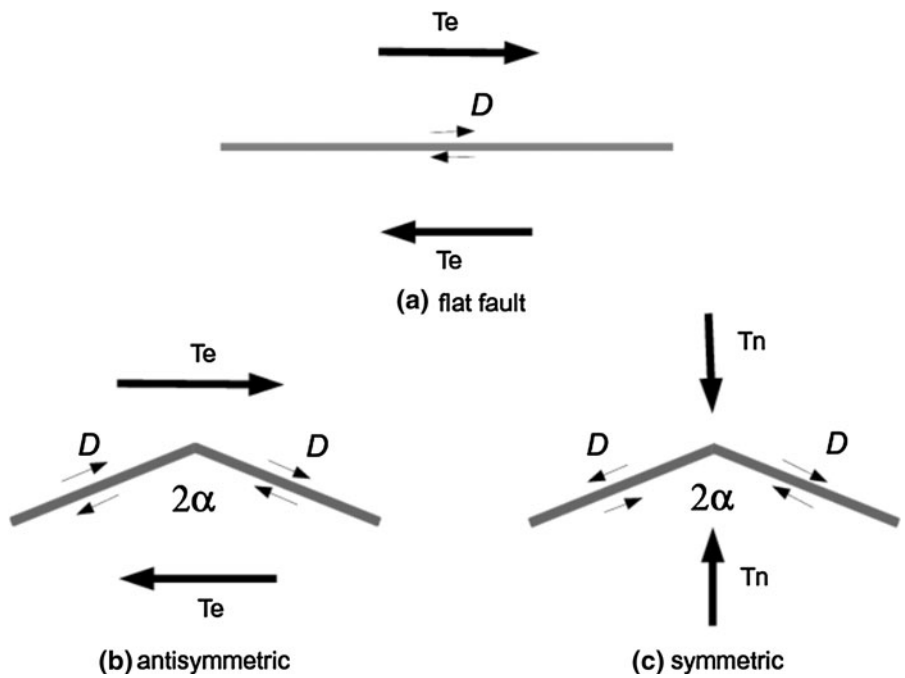

Figure 2
Geometry of the frictionless crack with a kink. In the reference model (**a**) the fault is flat and loaded by a uniform pure shear stress field. In models (**b**) and (**c**) the two sides of the kink make an angle $2\alpha(\alpha = \pi/2 - \Psi)$. In the antisymmetric case, the load is the same as for the flat model so that slip has the orientation shown in the picture. For model (**c**) the fault is loaded by uniaxial compression so that the load is symmetric on the two sides of the kink

$$u_r(r,\theta) = r^{\lambda}[A\cos((1+\lambda)\theta) + C\cos((1-\lambda)\theta)] \tag{20}$$

$$u_r(r,\phi) = r^{\lambda}[a\cos((1+\lambda)\phi) + c\cos((1-\lambda)\phi)], \tag{21}$$

with $\theta \in (-\alpha, \alpha)$ and $\phi \in (-\beta, \beta)$ respectively. Under symmetric load the two sides of the kink slip in opposite directions, so that the normal stress becomes singular at the origin. The singularity decreases linearly from 1 for small angles Ψ. The eigenvalues for symmetric load are shown in Fig. 3.

The antisymmetric solution has $\tilde{D} \neq 0$, and its associated eigenvalue equation is:

$$0 = \cos(\lambda\pi) - \cos(2\Psi)\cos(2\Psi\lambda) + \lambda\sin(2\Psi)\sin(2\Psi\lambda). \tag{22}$$

The eigenvalues for antisymmetric load are shown in Fig. 4. Antisymmetric load is what we expect for shear slip along two faults joined at a kink. Shear slip is continuous at the corner while the normal displacement changes sign producing a rotation of the cusp of the kink. Shear stress is continuous at the kink, but normal stress is discontinuous, one side being under compression, the other under tension. This jump in stress is a serious problem that needs to be carefully taken into account in the numerical simulations of kinks: indeed this solution on its own becomes unphysical under our assumptions of contact on all sides of the kink, since the fault cannot sustain tension. As we will see in the next section, the jump in normal stress persists when friction $f \neq 0$ for solutions that one can identify with these antisymmetric modes.

Ruling out the antisymmetric solution due to our assumption of contact, we observe from Fig. 3 that in the absence of friction and for small values of the kink angle Ψ and up to $\Psi_l = \arcsin(1/\sqrt{3}) \simeq 0.62$ the stress field near the cusp is dominated by the symmetric mode since the eigenvalue is between 0.5 and 1. On the other hand, at the limit angle, $\Psi_l \simeq 0.62$, the shear mode has a singularity with $\lambda = 0.5$ so that the cusp's singularity becomes like a crack tip's singularity. For larger kink angles, the symmetric mode should be ruled out under our assumptions, since it falls into the unphysical region of a too large singularity.

2.4.2 *Special Case, Both Sides of the Kink about to Slide Under Symmetric Shear Friction*

Let us now consider a kink where the cracks are under friction ($f \neq 0$), and are about to slide in the same way on both sides of the kink. In this case $w = -1$, and the modes decouple into simpler ones

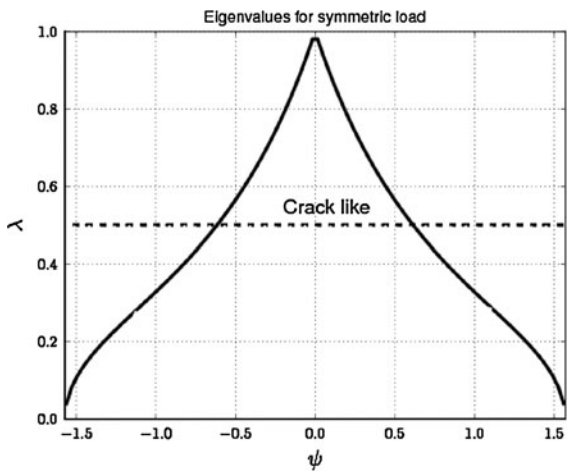

Figure 3
Eigenvalues for a simple frictionless crack under symmetric load (uniaxial compression). The eigenvalues $\lambda < 0.5$ are very unlikely to be excited because strain energy near the cusp would be unbounded. Thus, for angles between $-0.62 < \Psi < 0.62$ solutions are singular near the cusp

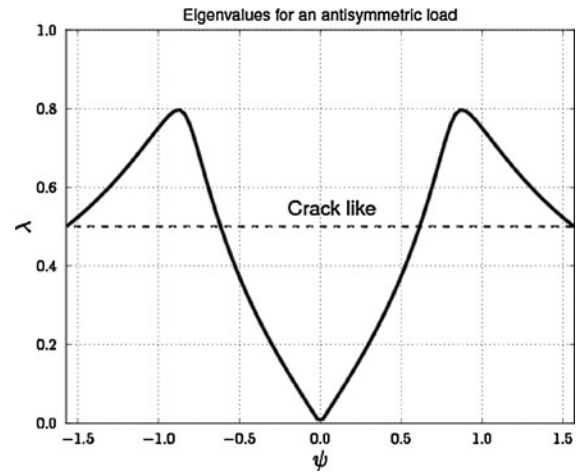

Figure 4
Eigenvalues for a simple frictionless crack under antisymmetric load (pure shear). The eigenvalues $\lambda < 0.5$ are very unlikely to be excited because strain energy near the cusp would be unbounded. Thus, for angles between $-0.62 < \Psi < 0.62$ solutions are regular near the cusp

like in the frictionless case of the previous section: the off-diagonal terms in the matrix of Eq. 52 are zero so that the eigenvalue equation splits into two.

The first equation is obtained setting $\tilde{D} = 0$ and $\tilde{C} \neq 0$, and its associated exponent solves the following equation:

$$0 = \cos(\lambda\pi) + \cos(2\Psi)\cos(2\Psi\lambda) - \lambda\sin(2\Psi)\sin(2\Psi\lambda) + f(1+\lambda)\sin(2\Psi)\cos(2\Psi\lambda), \quad (23)$$

these are symmetric modes which are very similar to those computed for a frictionless crack in the previous section (Eqs. 20 and 21). The main difference is that now the shear and normal stresses satisfy the friction law, Eq. 9. For the symmetric mode slip orientation again corresponds to that of Fig. 2c. At the cusp the slip directions are in the same radial direction producing a strong stress concentration so that the normal and shear stresses are singular with an exponent $\lambda < 1$ for small angles Ψ. All other properties are the same as for the frictionless case.

The other solution has $\tilde{C} = 0$ and $\tilde{D} \neq 0$, and its associated eigenvalue equation is:

$$0 = \cos(\lambda\pi) - \cos(2\Psi)\cos(2\Psi\lambda) + \lambda\sin(2\Psi)\sin(2\Psi\lambda) - f(1+\lambda)\sin(2\Psi)\cos(2\Psi\lambda), \quad (24)$$

these are antisymmetric modes similar to those of the frictionless crack discussed above, and we rule them out due to our assumption of contact. The symmetric and antisymmetric eigenvalues are plotted in Fig. 5.

2.5. *Method to Determine Possible Eigenvalue Solutions in the Complex Plane*

For fixed parameters Ψ, w and f, the eigenvalue equation (55) is a transcendental analytic function of λ equated to zero (it can be written as $g(\lambda, \Psi, w, f) = 0$). Thus, one can use results of analytic functions theory in order to analyze its number of zeroes (Long and Jiang, 1998).

The theory goes as following. In the next integral expression:

$$n = \frac{1}{2\pi i}\oint_C d\lambda \frac{g'(\lambda)}{g(\lambda)} \quad (25)$$

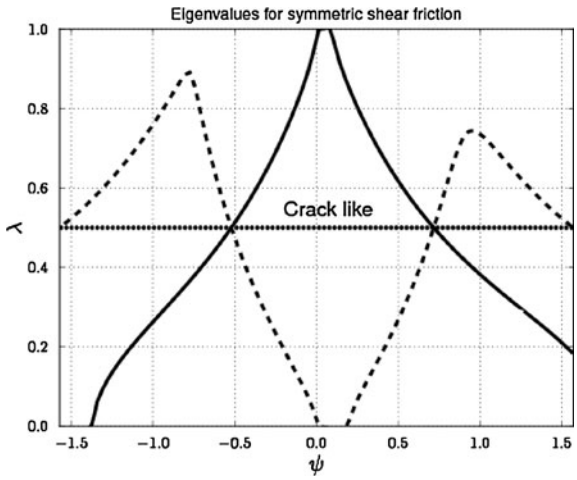

Figure 5
Eigenvalues for a kink under symmetric shear friction. The *continuous line* shows the symmetric eigenfunctions and the *broken line* shows the antisymmetric ones. The eigenvalues $\lambda < 0.5$ are very unlikely to be excited because strain energy near the cusp would be unbounded

n corresponds to the number of zeros of the function $g(\lambda)$ inside the arbitrary closed contour C (more accurately, in general it corresponds to the number of zeros minus the number of poles). Furthermore,

$$\sum_j \lambda_j = \frac{1}{2\pi i}\oint_C d\lambda\lambda \frac{g'(\lambda)}{g(\lambda)} \quad (26)$$

with λ_j a zero of g in the interior of C. Also,

$$\sum_j \lambda_j^2 = \frac{1}{2\pi i}\oint_C d\lambda\lambda^2 \frac{g'(\lambda)}{g(\lambda)}. \quad (27)$$

These equations allow us to determine the number of zeroes of $g(\lambda)$ in a given region of the complex λ space (notice that some of the zeroes could be complex), and their numerical values (this is easily seen when there are only two roots, and also notice that $g(\lambda)$ is an even function of λ for zero friction).

We applied these theoretical results using a contour in the λ plane which is a rectangle with vertical sides at $Re(\lambda) = 0.5$, 1 and horizontal sides variable (going to infinity in principle): this is the region of interesting singular solutions. The results are consistent with the fact that the only solutions in this region correspond to real solutions for λ, solutions that will be presented in the next section.

2.6. *General Numerical Solutions of Eigenvalue Equations*

We looked for numerical solutions of the eigenvalue equation (55) for the singular solution exponent λ under general frictional conditions near the cusp, and in the region $0.5 \leq Re(\lambda) < 1$ (the solutions turned out to be all real, as explained in the previous section). The following are plots that show solutions with λ real: they are obtained as contour plots at level zero of a function $g(\lambda, \Psi, w, f)$ with a choice of parameters, $f = 0.4$ and varying w (notice that the eigenvalue equation (55) is written as $g(\lambda, \Psi, w, f) = 0$). Figure 6 shows 2D contour plots with the friction coefficient f chosen as 0.4,w taken in the four cases as -1.0, -0.5, 0.5 and 1.0 respectively, Ψ between 0, $\pi/2$ and $\lambda \in (0.5, 1.0)$ (the range of interest). Notice that the plot corresponding to $w = -1.0$ corresponds to the special case with both sides about to slide under symmetric shear that was already presented: in this case we have shown the roots of the antisymmetric modes with shaded lines. As w changes in the following plots (to $w = -0.5$, 0.5 and 1.0) one sees a recognizable change of the $w = -1$ curves, i.e. one can associate the curves with their symmetric and antisymmetric origins.

Also, Fig. 7 shows plots of the strength of the normal stress on both sides of the kink (this is the prefactor of the normal stress, there is a radial variation on top of it), corresponding to the physical roots, λ, found on the previous figures, i.e. with friction coefficient f chosen as 0.4,w taken in the 4 cases as

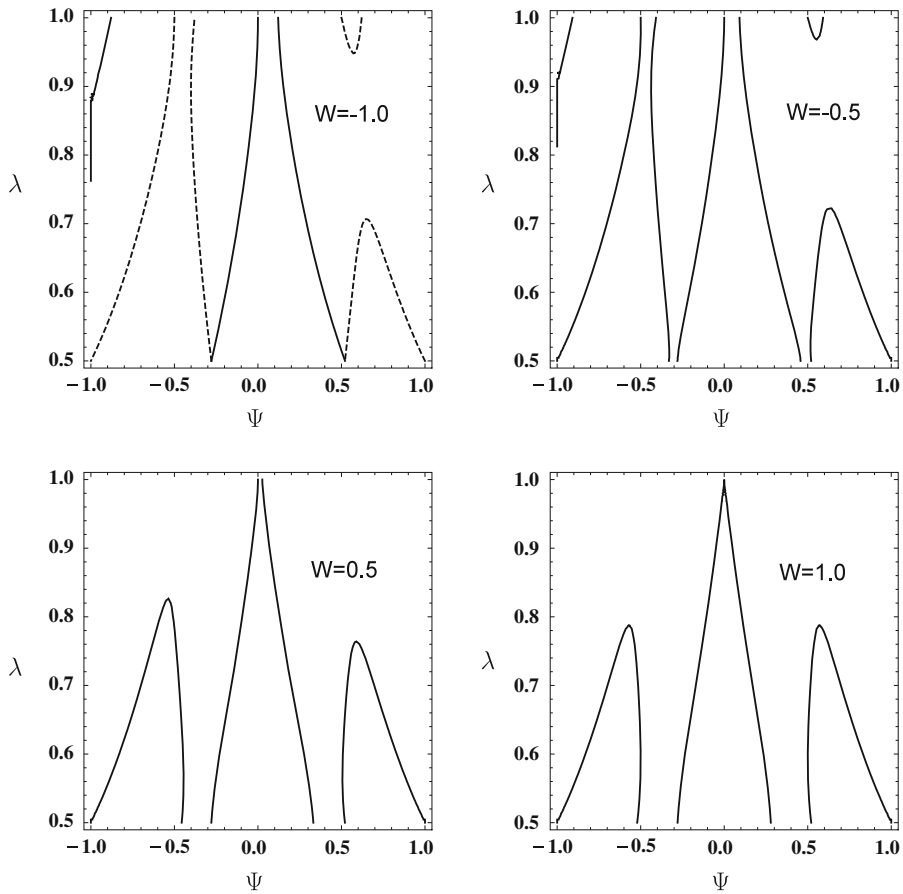

Figure 6
Roots of the eigenvalue equation for the radial exponent λ as a function of the angle Ψ, for four choices of the w coefficient. $f = 0.4$ and $w = -1.0$, -0.5, 0.5 and 1.0 for each successive plot

-1.0, -0.5, 0.5 and 1.0 respectively: these curves correspond to the curves on Fig. 6 that are or can be associated with the symmetric modes of $w = -1.0$. Indeed with these plots of Fig. 7 one sees that the normal stress has the same sign on both sides of the kink for all values of λ concerned, meaning that they correspond to contact modes, i.e. they are consistent with our assumption of faults under compression. As w differs from $w = -1.0$ these modes become of mixed character, but as far as the sign of the normal stress on both sides of the kink, it remains the same, i.e. one could say that the symmetric part prevails on them.

Notice that the modes that one can associate to the antisymmetric modes of $w = -1$ as one changes w, even though they get mixed character as w changes, the normal stress differs always in sign along both sides of the kink meaning that the assumption of contact cannot be sustained since the faults cannot sustain tension (in this sense one can say that they retain mainly an antisymmetric character).

All our numerical calculations were done with Poisson's ratio taken as $\nu = 0.3$.

Our Fig. 8 are polar plots of $\sigma_{\theta\theta}$ and $\sigma_{\phi\phi}$ for some allowed solutions, i.e. they reflect the angular variation of these stresses for specific parameters. We chose $f = 0.4$, $\alpha = 0.8$ $(\pi/2)$, $w = -1.0$ for the upper plot and $w = 0.5$ for the lower. The angles θ and ϕ range from 0 to α and from 0 to $\beta = \pi - \alpha$ (another way of thinking about the plot is to take θ to

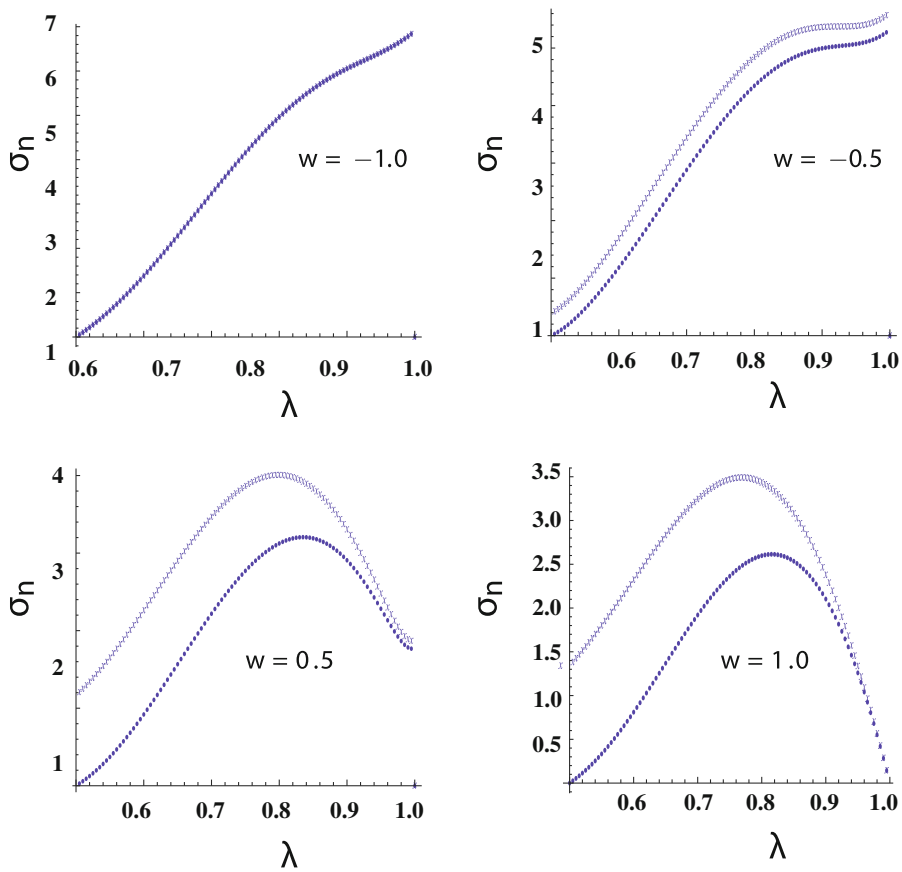

Figure 7
Amplitude of the normal stress along the two branches of the kink (in arbitrary units) as a function of the singular exponent λ for four choices of the w coefficient. $f = 0.4$ and $w = -1.0$, -0.5, 0.5 and 1.0 for each successive plot

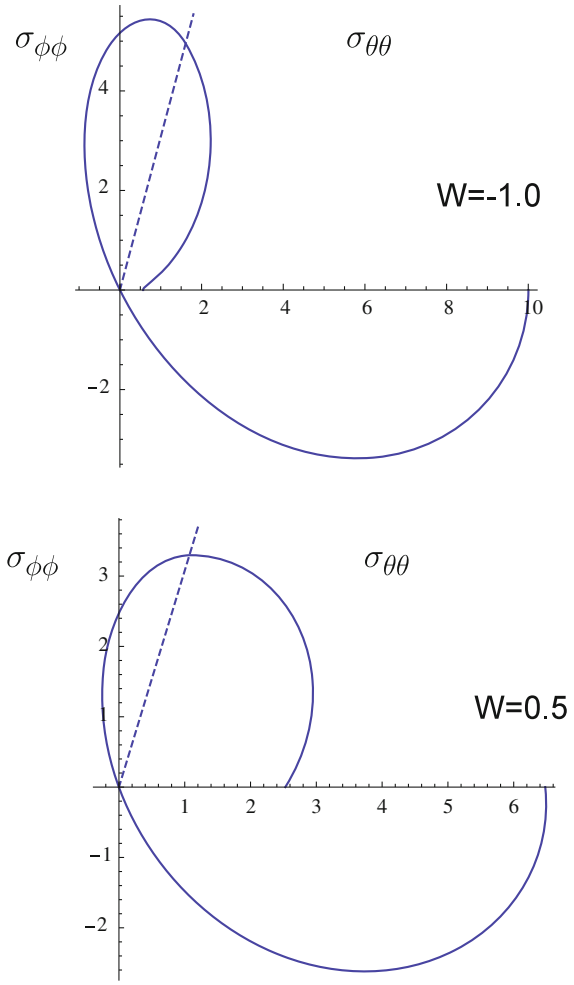

Figure 8
Polar plots of the amplitude of the stresses $\sigma_{\theta\theta}$ and $\sigma_{\phi\ \phi}$ of allowed solutions, as a function of angles in the upper region (i.e. $0 < \theta < \alpha = 0.8(\pi/2)$ and $0 < \phi < 1.2(\pi/2)$). The dashed line represents the fault, i.e. there $\theta = \alpha$. The other parameters that define the solutions are $f = 0.4$,$w = -1.0$ for the upper plot and $w = 0.5$ for the lower

range from 0 to π, and in the left region $\sigma_{\phi\phi}$ is equal to $\sigma_{\theta\theta}$). One clearly sees the continuity of the normal stress across the upper fault.

3. *Discussion and Conclusions*

Although fault geometry was recognized as a very important feature controlling rupture propagation and stress field in the vicinity of faults long ago, its effect remains largely ignored in most studies of earthquake dynamics. In order to fully understand the effects of geometry we need to solve a few canonical problems that illustrate the most important features of seismic rupture interaction with fault geometry. In this paper we looked at the static field in the vicinity of the cusp of a kink that does not open (mode I is not allowed). We considered a very general situation where one side of the kink, the lower one in Fig. 1, has already slipped (or is about to slip) and the other side is in a general mechanical state given by Eq. 9.

These equations allow us to understand the state of stress near the kink under very general load. We assume that there is no localized source in the vicinity of the kink, so that slip is due to the relaxation of the fault due to far field stress loading. In that case the minimum acceptable value for λ is 0.5. This is the stress field in the vicinity of a crack tip. For lower values of λ, strain energy is not finite and, therefore, an external source must be active at the cusp.

Assuming that the two sides of the fault are in a stress state such that on both the shear stress is exactly equal to the normal stress times the friction coefficient we found two modes of slip shown in Fig. 2. The two sides may be at the same frictional state under two circumstances: (1) the stress field is the same on both sides and both are ready to slip. In that case friction $f = f_s$ where f_s is the static friction; (2) the fault has just slipped so that friction $f = f_d$ where f_d is the dynamic friction stress coefficient. In this case the most singular state of stress is the symmetric load of Fig. 2 where the two sides slip in opposite directions.

In general, the friction coefficient or the load on both sides of the kink will be different. In that case the stress field will be of a mixed character, i.e. each mode is a combination of symmetric and antisymmetric loads, as shown in Fig. 7. For small angles Ψ those modes are dominated by a quasi-symmetric mode in which a stress singularity develops at the corner. Slip tries to pull the kink to open or to close even more tightly producing a singularity that is integrable. We allowed in our expressions for a broad range of practical situations that can be modelled using the variable w. For instance, differences in friction on both sides of the kink can be modelled using $w > -1$. Differences in load on the two sides of the kink can also be handled with different values of w.

Another important issue is that when the stress field near the corner is strictly antisymmetric, the stress field is discontinuous at the corner, one side being under increased tension and the other under increased compression. This produces a rotation of the cusp and has an influence on the seismic moment of the kinked crack. This type of mode, i.e. antisymmetric or close to it is ruled out under our model that assumes contact, since the faults cannot sustain tension. Thus, this feature will be further studied for a finite crack with a kink in future work, allowing for open regions of the faults.

The results presented here provide a general framework to study the static stress and displacement fields in the vicinity of a kink on a shear fault. They can be used to interpret numerical results obtained using boundary integral or finite element approaches or, as we expect, they can be used to create particular elements that better resolve the stress field at the kink.

Acknowledgments

The authors acknowledge financial support from project ECOS-CONICYT C06U02.

Appendix

Frictionless Boundary Conditions

We handle separately the boundary conditions, Eqs. 5–7, that are independent of friction since these allow us to reduce the number of unknowns. These lead to the following set of equations:

$$0 = \begin{pmatrix} \sin(1+\lambda)\beta & v_2\sin(1-\lambda)\beta & \sin(1+\lambda)\alpha & v_2\sin(1-\lambda)\alpha \\ \delta\sin(1+\lambda)\beta & \epsilon\sin(1-\lambda)\beta & \delta\sin(1+\lambda)\alpha & \epsilon\sin(1-\lambda)\alpha \\ \delta\cos(1+\lambda)\beta & \gamma\cos(1-\lambda)\beta & -\delta\cos(1+\lambda)\alpha & -\gamma\cos(1-\lambda)\alpha \end{pmatrix} \begin{pmatrix} a \\ c \\ A \\ C \end{pmatrix} \tag{28}$$

$$0 = \begin{pmatrix} \cos(1+\lambda)\beta & v_2\cos(1-\lambda)\beta & \cos(1+\lambda)\alpha & v_2\cos(1-\lambda)\alpha \\ \delta\cos(1+\lambda)\beta & \epsilon\cos(1-\lambda)\beta & \delta\cos(1+\lambda)\alpha & \epsilon\cos(1-\lambda)\alpha \\ \delta\sin(1+\lambda)\beta & \gamma\sin(1-\lambda)\beta & -\delta\sin(1+\lambda)\alpha & -\gamma\sin(1-\lambda)\alpha \end{pmatrix} \begin{pmatrix} b \\ d \\ B \\ D \end{pmatrix} \tag{29}$$

with

$$\gamma \equiv (1+\lambda)(1-v_2); \quad \delta \equiv 2\lambda; \quad \epsilon \equiv (1-\lambda)(1-v_2) \tag{30}$$

Manipulating these equations, and using that $\alpha + \beta = \pi$, one gets:

$$\begin{pmatrix} A \\ a \end{pmatrix} = \frac{1}{\delta\sin(\lambda\pi)} \begin{pmatrix} P(\beta) & Q(\alpha,\beta) \\ Q(\beta,\alpha) & P(\alpha) \end{pmatrix} \begin{pmatrix} c \\ C \end{pmatrix} \tag{31}$$

with

$$P(\beta) \equiv v_2\delta\cos((1+\lambda)\beta)\sin((1-\lambda)\beta) - \gamma\sin((1+\lambda)\beta)\cos((1-\lambda)\beta) \tag{32}$$

$$Q(\alpha,\beta) \equiv v_2\delta\cos((1+\lambda)\beta)\sin((1-\lambda)\alpha) + \gamma\sin((1+\lambda)\beta)\cos((1-\lambda)\alpha) \tag{33}$$

and

$$\begin{pmatrix} B \\ b \end{pmatrix} = \frac{1}{\delta \sin(\lambda\pi)} \begin{pmatrix} R(\beta) & S(\alpha,\beta) \\ S(\beta,\alpha) & R(\alpha) \end{pmatrix} \begin{pmatrix} d \\ D \end{pmatrix} \quad (34)$$

with

$$R(\beta) \equiv v_2\delta\sin((1+\lambda)\beta)\cos((1-\lambda)\beta) - \gamma\cos((1+\lambda)\beta)\sin((1-\lambda)\beta) \quad (35)$$

$$S(\alpha,\beta) \equiv v_2\delta\sin((1+\lambda)\beta)\cos((1-\lambda)\alpha) + \gamma\cos((1+\lambda)\beta)\sin((1-\lambda)\alpha) \quad (36)$$

Thus, one has obtained expressions for $A = A(c, C)$, $a = a(c, C)$, $B = B(d, D)$ and $b = b(d, D)$.

Boundary Conditions Involving Friction

The friction boundary conditions, Eqs. 8 and 9 become:

$$\begin{aligned} 0 = {} & \delta[\sin((1+\lambda)\alpha) + f\cos((1+\lambda)\alpha)]A \\ & + \delta[\cos((1+\lambda)\alpha) - f\sin((1+\lambda)\alpha)]B \\ & + [\epsilon\sin((1-\lambda)\alpha) + f\gamma\cos((1-\lambda)\alpha)]C \\ & + [\epsilon\cos((1-\lambda)\alpha) - f\gamma\sin((1-\lambda)\alpha)]D \end{aligned} \quad (37)$$

$$\begin{aligned} 0 = {} & \delta[\sin((1+\lambda)\alpha) - wf\cos((1+\lambda)\alpha)]A \\ & - \delta[\cos((1+\lambda)\alpha) + wf\sin((1+\lambda)\alpha)]B \\ & + [\epsilon\sin((1-\lambda)\alpha) - wf\gamma\cos((1-\lambda)\alpha)]C \\ & - [\epsilon\cos((1-\lambda)\alpha) + wf\gamma\sin((1-\lambda)\alpha)]D \end{aligned} \quad (38)$$

$$\begin{aligned} 0 = {} & \delta[\sin((1+\lambda)\beta) - f\cos((1+\lambda)\beta)]a \\ & + \delta[\cos((1+\lambda)\beta) + f\sin((1+\lambda)\beta)]b \\ & + [\epsilon\sin((1-\lambda)\beta) - f\gamma\cos((1-\lambda)\beta)]c \\ & + [\epsilon\cos((1-\lambda)\beta) + f\gamma\sin((1-\lambda)\beta)]d \end{aligned} \quad (39)$$

$$\begin{aligned} 0 = {} & \delta[\sin((1+\lambda)\beta) + wf\cos((1+\lambda)\beta)]a \\ & - \delta[\cos((1+\lambda)\beta) - wf\sin((1+\lambda)\beta)]b \\ & + [\epsilon\sin((1-\lambda)\beta) + wf\gamma\cos((1-\lambda)\beta)]c \\ & - [\epsilon\cos((1-\lambda)\beta) - wf\gamma\sin((1-\lambda)\beta)]d \end{aligned} \quad (40)$$

Furthermore, summing and subtracting Eqs. 37, 38 and 39, 40 one obtains:

$$\begin{aligned} 0 = {} & \delta[2\sin((1+\lambda)\alpha) + f(1-w)\cos((1+\lambda)\alpha)]A \\ & - f(1+w)\delta\sin((1+\lambda)\alpha)B \\ & + [2\epsilon\sin((1-\lambda)\alpha) + f(1-w)\gamma\cos((1-\lambda)\alpha)]C \\ & - f(1+w)\gamma\sin((1-\lambda)\alpha)]D \end{aligned} \quad (41)$$

$$\begin{aligned} 0 = {} & -f(1+w)\delta\cos((1+\lambda)\alpha)A - \delta[2\cos((1+\lambda)\alpha) \\ & - f(1-w)\sin((1+\lambda)\alpha)]B \\ & - f(1+w)\gamma\cos((1-\lambda)\alpha)]C - [2\epsilon\cos((1-\lambda)\alpha) \\ & - f(1-w)\gamma\sin((1-\lambda)\alpha)]D \end{aligned} \quad (42)$$

$$\begin{aligned} 0 = {} & \delta[2\sin((1+\lambda)\beta) - f(1-w)\cos((1+\lambda)\beta)]a \\ & + f(w+1)\delta\sin((1+\lambda)\beta)b \\ & + [2\epsilon\sin((1-\lambda)\beta) - f(1-w)\gamma\cos((1-\lambda)\beta)]c \\ & + f(w+1)\gamma\sin((1-\lambda)\beta)d \end{aligned} \quad (43)$$

$$\begin{aligned} 0 = {} & f(w+1)\delta\cos((1+\lambda)\beta)a - \delta[2\cos((1+\lambda)\beta) \\ & + f(1-w)\sin((1+\lambda)\beta)]b \\ & + f(w+1)\gamma\cos((1-\lambda)\beta)]c - [2\epsilon\cos((1-\lambda)\beta) \\ & + f(1-w)\gamma\sin((1-\lambda)\beta)]d \end{aligned} \quad (44)$$

After summing Eqs. 41 and 43 and replacing Eqs. 31 and 34 in them, one obtains:

$$\begin{aligned} 0 = {} & (\epsilon - v_2\delta)\sin(\lambda\pi)[\sin((1-\lambda)\beta)c \\ & + \sin((1-\lambda)\alpha)C] \end{aligned} \quad (45)$$

Similarly, summing Eqs. 42 and 44 and replacing Eqs. 31 and 34 in them, one obtains:

$$\begin{aligned} 0 = {} & (\epsilon - v_2\delta)\sin(\lambda\pi)[\cos((1-\lambda)\beta)d \\ & + \cos((1-\lambda)\alpha)D] \end{aligned} \quad (46)$$

In the derivation of Eqs. 45 and 46 we used the following identities:

$$\sin((1+\lambda)\beta)Q(\beta,\alpha) + \sin((1+\lambda)\alpha)P(\beta) = -v_2\delta\sin((1-\lambda)\beta)\sin(\lambda\pi) \quad (47)$$

$$\sin((1+\lambda)\beta)S(\beta,\alpha) - \sin((1+\lambda)\alpha)R(\beta) = -\gamma\sin((1-\lambda)\beta)\sin(\lambda\pi) \quad (48)$$

$$\cos((1+\lambda)\beta)Q(\beta,\alpha) - \cos((1+\lambda)\alpha)P(\beta) = -\gamma\cos((1-\lambda)\beta)\sin(\lambda\pi) \quad (49)$$

$$\cos((1+\lambda)\beta)S(\beta,\alpha) + \cos((1+\lambda)\alpha)R(\beta) = -v_2\delta\cos((1-\lambda)\beta)\sin(\lambda\pi) \quad (50)$$

Eigenvalue Equation for the Singular Exponent and Eigenvector

We now show the final steps in order to get an eigenvalue equation that allows us to determine the singular solutions with their corresponding exponents λ.

From Eqs. 45 and 46 one can write:

$$\begin{aligned} c &= \sin((1-\lambda)\alpha)\tilde{C}; \quad C = -\sin((1-\lambda)\beta)\tilde{C} \\ d &= \cos((1-\lambda)\alpha)\tilde{D}; \quad D = -\cos((1-\lambda)\beta)\tilde{D} \end{aligned} \tag{51}$$

Replacing Eq. 51 into Eqs. 43 and 44, one gets [except for a pre-factor $(1-\nu_2)\sin(\lambda\pi)$]:

$$0 = \begin{pmatrix} \begin{pmatrix} 2\cos(\lambda\pi) \\ +2\cos(2\Psi)\cos(2\Psi\lambda) \\ -2\lambda\sin(2\Psi)\sin(2\Psi\lambda) \\ +f(1-w)(1+\lambda)\times \\ \sin(2\Psi)\cos(2\Psi\lambda) \end{pmatrix} & \begin{pmatrix} f(w+1)(1+\lambda)\times \\ \sin(2\Psi)\cos(2\Psi\lambda) \end{pmatrix} \\ \begin{pmatrix} -f(w+1)(1+\lambda)\times \\ \sin(2\Psi)\cos(2\Psi\lambda) \end{pmatrix} & \begin{pmatrix} 2\cos(\lambda\pi) \\ -2\cos(2\Psi)\cos(2\Psi\lambda) \\ +2\lambda\sin(2\Psi)\sin(2\Psi\lambda) \\ -f(1-w)(1+\lambda)\times \\ \sin(2\Psi)\cos(2\Psi\lambda) \end{pmatrix} \end{pmatrix} \begin{pmatrix} \tilde{C} \\ \tilde{D} \end{pmatrix} \tag{52}$$

where $\Psi \equiv (\beta-\alpha)/2$. The following relations were used:

$$\begin{aligned} &\sin((1-\lambda)\alpha)Q(\beta,\alpha) - \sin((1-\lambda)\beta)P(\alpha) \\ &\quad = \gamma\sin((1+\lambda)\alpha)\sin(\lambda\pi) \end{aligned} \tag{53}$$

$$\begin{aligned} &\cos((1-\lambda)\alpha)S(\beta,\alpha) - \cos((1-\lambda)\beta)R(\alpha) \\ &\quad = \gamma\cos((1+\lambda)\alpha)\sin(\lambda\pi) \end{aligned} \tag{54}$$

It follows that the equation for the exponent λ of the singular solutions corresponds to the determinant of the previous matrix equated to zero:

$$\begin{aligned} 0 = {} & 4\cos^2(\lambda\pi) + [f(w+1)(1+\lambda)\sin(2\Psi)\cos(2\Psi\lambda)]^2 \\ & - [2\cos(2\Psi)\cos(2\Psi\lambda) - 2\lambda\sin(2\Psi)\sin(2\Psi\lambda) \\ & + f(1-w)(1+\lambda)\sin(2\Psi)\cos(2\Psi\lambda)]^2 \end{aligned} \tag{55}$$

References

Adda-Bedia, M. and Arias, R. (2003), *Brittle fracture dynamics with arbitrary paths–I. Dynamic crack kinking under general antiplane loading*, J. Mech. Phys. Solids, *51*, 1287–1304.

Adda-Bedia, M. and Madariaga, R. (2008), *Seismic radiation from a kink on an antiplane fault*, Bull. Seismol. Soc. Am., *98*, 2291–2302.

Andrews, D. J. (1989), *Mechanics of fault junctions*, J. Geophys. Res., *94*, 9389–9397.

Aochi, H., Fukuyama, E. and Matsu'ura M. (2000), *Spontaneous rupture propagation on a non-planar fault in 3-D elastic medium*, Pure Appl. Geophys. *157*, 2003–2027.

Barenblatt, G. I. (1996), *Scaling, self-similarity and intermediate asymptotics*, (Cambridge University Press, Cambridge, U.K.).

Bouchbinder, E., Livne, A. and J. Fineberg, J. (2009), *The 1/r singularity in weakly nonlinear fracture mechanics* J. Mech. Phys. Solids., *57*, 1568–1577.

Harris, R. A. and Day, S. (1999), *Dynamic 3D simulations of earthquakes on an echelon faults*, Geophys. Res. Lett., *26*, 2089–2092.

Kame, N., Rice, J.R. and Dmowska, R. (2003), *Effects of prestress state and rupture velocity on dynamic fault branching*, J. Geophys. Res., *108*, 2265, doi:10.1029/2002JGB002189.

Kame, N. and Yamashita, T. (1999), *Simulations of the spontaneous growth of a dynamic crack without constraints on the crack tip path*. Geophys. J. Int., *130*, 345–358.

Kame, N. and Yamashita, T. (2003), *Dynamic branching, arresting of rupture and the seismic wave radiation in self-chosen crack path modelling*, Geophys. J. Int., *155*, 1042–1050.

King, G. and Nabelek, J. (1985), *The role of bends in faults in the initiation and termination of earthquake rupture*, Science, *228*, 984–987.

Labossiere, P.E.W. and Dunn, M. L. (2001) *Fracture initiation at three-dimensional bimaterial interface corners*. J. Mech. Phys. Solids, *49*, 609–634

Long, Y. and Jiang, H. (1998), *Rigorous numerical solution to complex transcendental equations*, Int. Journal Infrared Millimiter Waves, *19*, 785-790.

Oglesby, D.D., Day, S. M., LI, Y-G. and Vidale, J. E. (2003), *The 1999 Hector Mine earthquake: the dynamics of a branched fault system*, Bull. Seismol. Soc. Am., *93*, 2459–2476.

Poliakov, A., Dmowska, R. and Rice, J.R. (2002), *Dynamic shear rupture interactions with fault bends and off-axis secondary faulting*, J. Geophys. Res., *107*, 2295, doi:10.1029/2001JB000572.

Seweryn, A. and Molski, K. (1996), *Elastic stress singularities and corresponding generalized stress intensity factors for angular corners under various boundary conditions*. Eng. Fract. Mechanics, *55*, 529–556.

Segal, P. and Pollard, D. D. (1980), *Mechanics of discontinuous faults*, J. Geophys. Res., *85*, 4337–4350.

Sibson, R. H. (1985), *Stopping of earthquake ruptures at dilatational fault jogs*, Nature, *316*, 248–251.

Sih, G. C. (1965). *Stress distribution near internal crack tips for longitudinal shear problems*, J. Appl. Mech. *32*, 51–58.

Tada, T. and Yamashita, K. (1997), *The paradox of smooth and abrupt bends in two-dimensional in-plane shear-crack mechanics Geophys*. J. Int., *127*, 795–800, 1997.

Williams, M. L. (1952), *Stress singularities resulting from various boundary conditions in angular corners of plates in extension*, J. Applied Mech., *19*, 526–534.

(Received August 8, 2010, revised January 30, 2011, accepted February 1, 2011, Published online March 11, 2011)